

Overcoming the sign problem in one-dimensional QCD by new integration rules with polynomial exactness

A. Ammon,^{4,*} T. Hartung,^{2,†} K. Jansen,^{1,‡} H. Leövey,^{3,§} and J. Volmer^{1,||}

¹*NIC, DESY Zeuthen, Platanenallee 6, 15738 Zeuthen, Germany*

²*Department of Mathematics, King's College London, Strand, London WC2R 2LS, United Kingdom*

³*Institut für Mathematik, Humboldt-Universität zu Berlin, Unter den Linden 6, 10099 Berlin, Germany*

⁴*IVU Traffic Technologies AG, Bundesallee 88, 12161 Berlin, Germany*

(Received 12 August 2016; published 9 December 2016)

In this paper we describe a new integration method for the groups $U(N)$ and $SU(N)$, for which we verified numerically that it is polynomially exact for $N \leq 3$. The method is applied to the example of one-dimensional QCD with a chemical potential. We explore, in particular, regions of the parameter space in which the sign problem appears due to the presence of the chemical potential. While Markov chain Monte Carlo fails in this region, our new integration method still provides results for the chiral condensate on arbitrary precision, demonstrating clearly that it overcomes the sign problem. Furthermore, we demonstrate that also in other regions of parameter space our new method leads to errors which are reduced by orders of magnitude.

DOI: [10.1103/PhysRevD.94.114508](https://doi.org/10.1103/PhysRevD.94.114508)

I. INTRODUCTION

The sign problem in models of statistical and high-energy physics constitutes one of the greatest challenges for computational sciences, because of the difficulty of evaluating such systems [1]. Many attempts using various techniques have been developed but no general solution to overcome the sign problem has been found so far [2]. On the other hand, the sign problem appears in important problems in physics. For example, in high-energy physics, the sign problem prevents the full understanding of the physics of the early Universe and the explaining and interpreting of heavy ion collisions. In order to progress with these questions, simulations within the framework of lattice QCD with a nonzero chemical potential would be required. However, these are impossible with present techniques; see Refs. [3,4] for recent reviews. The reason is that standard computations in lattice QCD employ Markov chain Monte Carlo (MC-MC) methods which need a positive integrand in order to be applicable. However, in the problem just mentioned a chemical potential is required, leading to a complex integrand and therefore to an oscillating function. In particular, if the sign cancellation errors due to the plural oscillations are of significantly higher magnitude than the real integral value, it becomes unfeasible to evaluate such systems.

Therefore, alternative approaches to MC-MC methods need to be developed and in [5,6] we have proposed and tested quasi-Monte Carlo and iterated numerical

integration techniques. These methods can improve the convergence of the involved integrations and also have the potential to deal with the sign problem. However, in this paper we discuss yet another method of numerical integration for generic systems with a sign problem. This new method leads to an arbitrarily precise evaluation of the involved integrals and is based on a complete symmetrization of the integrals considered.

This can be achieved through new integration rules on compact groups, as developed in this article, which lead to polynomial exactness. We test the method on the example of one-dimensional QCD with a chemical potential, see, e.g., [7], for which other approaches have already been used to solve the sign problem [8]. Although one-dimensional QCD is a model with an interest in its own as the strong coupling limit of QCD [9], we consider it here only as a benchmark model for testing our approach, especially since it is possible to compute observables analytically and, thus, check the numerical results directly. In particular, we will compute the chiral condensate for a broad range of action parameters, including values of the chemical potential that are impossible (for all practical purposes) to address with standard Monte Carlo techniques.

The idea to symmetrize the involved integrals in a MC-MC simulation to achieve positivity and stable results has also been proposed in Refs. [10,11]. However, in these works only an incomplete symmetrization has been used and still a large number of Monte Carlo samples were necessary to obtain accurate results. In our approach, we perform a polynomially exact integration avoiding the MC-MC step. This way, we only need a very small number of integration points. In fact, we can reach arbitrary (up to machine) precision for the targeted physical observables and avoid the MC error completely.

*andreas.ammon@desy.de

†tobias.hartung@kcl.ac.uk

‡karl.jansen@desy.de

§leovey@math.hu-berlin.de

||julia.volmer@desy.de

For our computations, we employ the compact groups $U(N)$ and $SU(N)$ and give a description for a complete symmetrization for $N \leq 3$. As we will demonstrate, for these cases with our new approach the sign problem is completely avoided.

This paper is composed in the following way: In Sec. II, we introduce the model of one-dimensional QCD, show analytic results of the partition function Z , and demonstrate the difficulty of computing Z for specific parameters numerically. In Sec. III, we describe the polynomially exact method based on completely symmetrized spherical

quadrature rules [12]. In Sec. IV, we explain our numerical computations in more detail, show results for the partition function and the chiral condensate, and explain their behavior for different parameter values. In Sec. V, we finally conclude the paper.

II. ONE-DIMENSIONAL LATTICE QCD

Let us consider the following Dirac operator (cf., e.g., [7]) for a lattice with n points

$$\mathfrak{D}(U) = \begin{pmatrix} m & \frac{e^\mu}{2} U_1 & & & & & \frac{e^{-\mu}}{2} U_n^* \\ -\frac{e^{-\mu}}{2} U_1^* & m & \frac{e^\mu}{2} U_2 & & & & \\ & -\frac{e^{-\mu}}{2} U_2^* & m & \frac{e^\mu}{2} U_3 & & & \\ & & & \ddots & \ddots & & \\ & & & & \ddots & \ddots & \\ -\frac{e^{-\mu}}{2} U_n & & & -\frac{e^{-\mu}}{2} U_{n-2}^* & m & \frac{e^{-\mu}}{2} U_{n-1} & \\ & & & & -\frac{e^{-\mu}}{2} U_{n-1}^* & m & \end{pmatrix} \quad (1)$$

where all empty entries are zero and the corresponding one-flavor partition function

$$Z(m, \mu, G, n) = \int_{G^n} \det \mathfrak{D}(U) dh_G^n(U) \quad (2)$$

where $G = U(N)$ or $G = SU(N)$, $N \in \mathbb{N}$, and h_G is the corresponding (normalized) Haar measure on G .

In order to reduce the numerical effort in calculating $\det \mathfrak{D}$, we will first reduce the dimension using the following theorem.

Theorem 1: Let $U_0 := U_n$, $\tilde{m}_1 := m$,

$$\forall j \in [2, n-1] \cap \mathbb{N}: \tilde{m}_j := m + \frac{1}{4\tilde{m}_{j-1}}, \quad (3)$$

and

$$\tilde{m}_n := m + \frac{1}{4\tilde{m}_{n-1}} + \sum_{j=1}^{n-1} \frac{(-1)^{j+1} 2^{-2j}}{\tilde{m}_j \prod_{k=1}^{j-1} \tilde{m}_k^2}. \quad (4)$$

Then,

$$\det \mathfrak{D} = \det \left(\prod_{j=1}^n \tilde{m}_j + 2^{-n} e^{-n\mu} \left(\prod_{j=0}^{n-1} U_j \right)^* + (-1)^n 2^{-n} e^{n\mu} \prod_{j=0}^{n-1} U_j \right). \quad (5)$$

The proof of this theorem can be found in Appendix A. In particular, in the gauge satisfying $U_j = 1$ except for $U_n = U$, Theorem 1 yields

$$\begin{aligned} \det \mathfrak{D} &= \det \left(\prod_{j=1}^n \tilde{m}_j + 2^{-n} e^{-n\mu} U^* + (-1)^n 2^{-n} e^{n\mu} U \right) \\ &= \det (c_1 + c_2 U^* + c_3 U), \end{aligned} \quad (6)$$

with $c_1 := \prod_{j=1}^n \tilde{m}_j$, $c_2 = 2^{-n} e^{-n\mu}$, and $c_3 = (-1)^n 2^{-n} e^{n\mu}$.

Mathematically speaking, (6) is an application of ‘‘Fubini’’¹ and translation invariance of the Haar measure since $\det \mathfrak{D}$ only depends on $\prod_{j=0}^{n-1} U_j$. We will frequently assume this form of \mathfrak{D} in analytic computations and we have implemented this form of \mathfrak{D} in order to reduce computational overhead. Similarly, c_1 , c_2 , and c_3 are standard notations in this paper. Since $U \in U(N)$ or $U \in SU(N)$ $\det \mathfrak{D}$ is a polynomial of degree N .

As an observable of the model, we investigate the chiral condensate

$$\begin{aligned} \chi(m, \mu, G, n) &= \partial_m \ln Z(m, \mu, G, n) \\ &= \frac{\partial_m Z(m, \mu, G, n)}{Z(m, \mu, G, n)} = \frac{\int_G \partial_m \det \mathfrak{D} dh_G}{\int_G \det \mathfrak{D} dh_G}. \end{aligned} \quad (7)$$

Since $\det \mathfrak{D}$ is a polynomial of degree N and the derivative ∂_m only acts on the term $\prod_{j=1}^n \tilde{m}_j$ in Theorem 1, $\partial_m \det \mathfrak{D}$ is still a polynomial of degree N and $\partial_m \prod_{j=1}^n \tilde{m}_j$ can be computed using symbolic differentiation.

¹Since all our groups are compact, they are unimodular and the Haar measures satisfy $h_{G \times H} = h_G \times h_H$ and $h_{G \rtimes H} = h_G \times h_H$ (cf., e.g., exercise 2.1.7 in [13]).

Theorem 2 not only allows us to reduce numerical overhead but we can furthermore calculate the partition function (2) (and therefore also the chiral condensate) analytically.

Theorem 2: Let $c_1 := \prod_{j=1}^n \tilde{m}_j$, $c_2 = 2^{-n} e^{-n\mu}$, and $c_3 = (-1)^n 2^{-n} e^{n\mu}$ with \tilde{m}_j as in Theorem 1. Then,

$$Z(m, \mu, U(1), n) = \int_{U(1)} \det \mathfrak{D}(U) dh_{U(1)}(U) = c_1, \quad (8)$$

$$\begin{aligned} Z(m, \mu, U(2), n) &= \int_{U(2)} \det \mathfrak{D}(U) dh_{U(2)}(U) \\ &= c_1^2 - c_2 c_3, \end{aligned} \quad (9)$$

$$\begin{aligned} Z(m, \mu, SU(2), n) &= \int_{SU(2)} \det \mathfrak{D}(U) dh_{SU(2)}(U) \\ &= c_1^2 + c_2^2 - c_2 c_3 + c_3^2, \end{aligned} \quad (10)$$

$$\begin{aligned} Z(m, \mu, U(3), n) &= \int_{U(3)} \det \mathfrak{D}(U) dh_{U(3)}(U) \\ &= c_1^3 - 2c_1 c_2 c_3, \end{aligned} \quad (11)$$

and

$$\begin{aligned} Z(m, \mu, SU(3), n) &= \int_{SU(3)} \det \mathfrak{D}(U) dh_{SU(3)}(U) \\ &= c_1^3 - 2c_1 c_2 c_3 + c_2^3 + c_3^3. \end{aligned} \quad (12)$$

For the proof of this theorem, see Appendix B.

In addition, we can deduce the behavior of Z for $m \searrow 0$.

Corollary 1: Let $\tilde{m}_1 := m$, $\tilde{m}_j := m + \frac{1}{4\tilde{m}_{j-1}}$, $\tilde{m}_n := m + \frac{1}{4\tilde{m}_{n-1}} + \sum_{j=1}^{n-1} \frac{(-1)^{j+1} 4^{-j}}{m \prod_{k=1}^{j-1} \tilde{m}_k \tilde{m}_{k+1}}$, and $c_1 := \prod_{j=1}^n \tilde{m}_j$. Then,

$$\lim_{m \searrow 0} c_1 = \begin{cases} 2^{1-n}, & n \in 2\mathbb{N} \\ 0, & n \in 2\mathbb{N} - 1 \end{cases}. \quad (13)$$

In particular,

$$\lim_{m \searrow 0} Z(m, \mu, U(1), n) = \begin{cases} 2^{1-n}, & n \in 2\mathbb{N} \\ 0, & n \in 2\mathbb{N} - 1 \end{cases}, \quad (14)$$

$$\lim_{m \searrow 0} Z(m, \mu, U(2), n) = \begin{cases} 3 \cdot 2^{-2n}, & n \in 2\mathbb{N} \\ -2^{-2n}, & n \in 2\mathbb{N} - 1 \end{cases}, \quad (15)$$

$$\begin{aligned} \lim_{m \searrow 0} Z(m, \mu, SU(2), n) &= \begin{cases} 3 \cdot 2^{-2n} + 2^{1-2n} \cosh(2n\mu), & n \in 2\mathbb{N} \\ 2^{1-2n} \sinh(2n\mu) - 2^{-2n}, & n \in 2\mathbb{N} - 1 \end{cases}, \end{aligned} \quad (16)$$

$$\lim_{m \searrow 0} Z(m, \mu, U(3), n) = \begin{cases} 4 \cdot 2^{-3n}, & n \in 2\mathbb{N} \\ 0, & n \in 2\mathbb{N} - 1 \end{cases}, \quad (17)$$

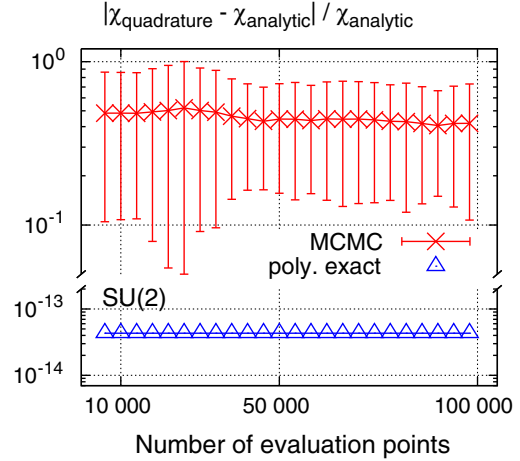


FIG. 1. Failure of MC-MC methods. Comparison of the relative error of the chiral condensate χ using polynomially exact (bottom) and Monte Carlo (top) quadrature rules for $SU(2)$. The polynomially exact rule used $n = 8$ integration points, $m = 0.25$, $\mu = 1.0$, and the error bars have been computed from 20 independent repetitions.

$$\begin{aligned} \lim_{m \searrow 0} Z(m, \mu, SU(3), n) &= \begin{cases} 4 \cdot 2^{-3n} + 2^{1-3n} \cosh(3n\mu), & n \in 2\mathbb{N} \\ 2^{1-3n} \sinh(3n\mu), & n \in 2\mathbb{N} - 1 \end{cases}. \end{aligned} \quad (18)$$

For the proof of this corollary, see Appendix C.

If $n\mu$ is large and m small, we can see clearly why the integrals in Theorem 2 are difficult to treat numerically, especially the $U(N)$ cases. If we assume a stochastic approach, e.g., a Monte Carlo method, then each evaluation of $\det \mathfrak{D}$ in the form (6) is a value in the vicinity of $|c_2|^N + |c_3|^N \approx |c_3|^N = 2^{-Nn} e^{Nn\mu}$.² However, performing the integration (or taking the limit of infinitely many samples), there is a very high degree of cancellations to be observed. Since discrete Markov chain Monte Carlo methods perform poorly with respect to such cancellations, they have to overcome an initial error in the vicinity of $e^{Nn\mu}$. In other words, as $n\mu$ grows larger, we need very good algorithms to suppress the initial error and the convergence

$$\text{error} \approx \frac{\text{constant}}{\sqrt{\text{sample size}}}$$

of Monte Carlo methods is simply not viable anymore. For example, in Fig. 1, we compare a Monte Carlo method (using reweighting) to our new, polynomially exact method proposed in Sec. III (details of the numerical tests can be found in Sec. IV). The error bars, the known rate of convergence $\frac{1}{\sqrt{\text{sample size}}}$, and the relative error of order 1

² $|c_2|^N + |c_3|^N = 2^{-Nn} e^{-Nn\mu} + |(-1)^{Nn} 2^{-Nn} e^{Nn\mu}| \approx 2^{-Nn} e^{Nn\mu} = |c_3|^N$, due to the fact that $e^x > e^{-x}$ for $x \in \mathbb{R}_{>0}$ and the (anti)symmetric shape of $e^x \pm e^{-x}$.

seen here show that the Monte Carlo method cannot reach the same level of precision with a reasonable number of samples (note the different scales for the Monte Carlo and polynomially exact results).

III. EFFICIENT QUADRATURE RULES OVER THE COMPACT GROUPS

Consider $Z(m, \mu, U(1), n)$ for the moment. As we have mentioned before, the problem is that the integral $\int_{U(1)} (-1)^{n-2^{-n}} e^{n\mu} U dh_{U(1)}(U)$ in (8) vanishes but the modulus of each evaluation $|(-1)^{n-2^{-n}} e^{n\mu} U|$ is large. However, if we were also to evaluate at $-U$ (or, more generally, at t equally spaced points along the unit circle), the two terms would cancel. However, the (geometric) idea of taking opposite points or equally spaced points on circles is not easy to formalize for $SU(N)$ and $U(N)$ with $N \geq 2$. Instead, we should note that the quadrature rule

$$\int_{U(1)} f(U) dh_{U(1)}(U) \approx \frac{1}{t+1} \sum_{k=1}^{t+1} f(e^{\frac{2\pi i k}{t+1}}) \quad (19)$$

is a spherical t -design (i.e., an equal-weight quadrature rule with spherical polynomial degree of exactness t ; cf. Example 5.14 in [14]). Since $\det \mathfrak{D}$ is a polynomial of degree N over the matrix entries for $U(N)$ and $SU(N)$, it suffices to consider t -designs or “weighted” t -designs (polynomially exact rules with possibly nonequal weights) with $t = N$.

In this section, we will discuss the construction of weighted t -designs for $N > 1$ and, especially, why we base the $U(N)$ and $SU(N)$ quadrature on the quadrature rules [12] for the spheres S^N .

Since

$$U(N) \cong SU(N) \rtimes U(1), \quad (20)$$

holds, where \rtimes denotes the (outer) semidirect product, we may construct a (weighted) t -design $Q_{U(N)}$ over $U(N)$ by considering two different (weighted) t -design rules $Q_{SU(N)}$

$$\Phi_2((\alpha, \varphi), U) = \begin{pmatrix} e^{i\alpha_1} \cos(\varphi_1) & 0 & e^{i\alpha_1} \sin(\varphi_1) \\ -e^{i\alpha_2} \sin(\varphi_1) \sin(\varphi_2) & e^{-i\alpha_1 - i\alpha_3} \cos(\varphi_2) & e^{i\alpha_2} \cos(\varphi_1) \sin(\varphi_2) \\ -e^{i\alpha_3} \sin(\varphi_1) \cos(\varphi_2) & -e^{-i\alpha_1 - i\alpha_2} \sin(\varphi_2) & e^{i\alpha_3} \cos(\varphi_1) \cos(\varphi_2) \end{pmatrix} \begin{pmatrix} U & 0 \\ 0 & 1 \end{pmatrix}, \quad (22)$$

whose restriction $\Phi_2: ([0, 2\pi]^3 \times (0, \frac{\pi}{2})^2) \times SU(2) \rightarrow SU(3)_1$ with

$$SU(3)_1 := \Phi_2([([0, 2\pi]^3 \times (0, \frac{\pi}{2})^2) \times SU(2)], \quad (23)$$

³More precisely, $SU(N)$ is a principal $SU(N-1)$ bundle over S^{2N-1} ; cf., e.g., Eq. (22.18) of [16].

and $Q_{U(1)}$ over $SU(N)$ and $U(1)$ correspondingly, and then define the product rule $Q_{U(N)} = Q_{SU(N)} \times Q_{U(1)}$. It is clear that by defining $Q_{U(N)}$ as a product rule in this way, we obtain a (weighted) t -design over $U(N)$. Since t -designs over $U(1)$ are easy to construct [see (19)], the entire problem of constructing (weighted) t -designs for the compact groups considered here reduces to the one of constructing (weighted) t -designs over $SU(N)$.

Starting with $SU(2)$, we have a measure preserving diffeomorphism $SU(2) \cong S^3$. An explicit mapping can be given by

$$\Phi: \mathbb{C}^2 \rightarrow \mathbb{C}^{2,2}; \quad (\alpha, \beta) \mapsto \begin{pmatrix} \alpha & -\beta^* \\ \beta & \alpha^* \end{pmatrix} \quad (21)$$

whose restriction $\Phi|_{S^3}^{SU(2)}: S^3 \rightarrow SU(2)$ is the mentioned measure preserving diffeomorphism. Thus, for this case we can resort to already well-known (weighted) t -designs over the 3-sphere (see [12,15]) for obtaining (weighted) t -designs over $SU(2)$ through the mapping Φ .

Moving on to $SU(3)$, we note that there is a correspondence³ between $SU(3)$ and $S^5 \times SU(2)$. More specifically, we consider first the covering $\Phi_1: [0, 2\pi]^3 \times [0, \frac{\pi}{2}]^2 \rightarrow S^5$ defined by

$$\begin{aligned} x_1 &= \cos(\alpha_1) \sin(\varphi_1) \\ x_2 &= \sin(\alpha_1) \sin(\varphi_1) \\ x_3 &= \sin(\alpha_2) \cos(\varphi_1) \sin(\varphi_2) \\ x_4 &= \cos(\alpha_2) \cos(\varphi_1) \sin(\varphi_2) \\ x_5 &= \sin(\alpha_3) \cos(\varphi_1) \cos(\varphi_2) \\ x_6 &= \cos(\alpha_3) \cos(\varphi_1) \cos(\varphi_2) \end{aligned}$$

and note that the restriction $\Phi_1: [0, 2\pi]^3 \times (0, \frac{\pi}{2})^2 \rightarrow S^5_1$, $S^5_1 := \Phi_1([0, 2\pi]^3 \times (0, \frac{\pi}{2})^2)$, is a diffeomorphism. Furthermore, the set $S^5_0 := S^5 \setminus S^5_1$ is a null set. On the other hand, we have the mapping $\Phi_2: ([0, 2\pi]^3 \times [0, \frac{\pi}{2}]^2) \times SU(2) \rightarrow SU(3)$ defined by

is a bijection and the set $SU(3)_0 := SU(3) \setminus SU(3)_1$ is a Haar null set. Thus, starting with a (weighted) t -design rule Q_{S^3} over S^3 and a (weighted) t -design $Q_{S^5_1}$ over S^5 , such that each point of $Q_{S^5_1}$ lies in S^5_1 , and considering the mapping

$$\Phi_3: S^5_1 \times S^3 \rightarrow SU(3); \quad (x, y) \mapsto \Phi_2(\Phi_1^{-1}(x), \Phi(y)), \quad (24)$$

we obtain a quadrature rule $Q_{SU(3)}$ over $SU(3)$ by setting $Q_{SU(3)} := \Phi_3[Q_{S_1^3} \times Q_{S^3}]$.

In fact, by considering (randomized) fully symmetric interpolatory rules $Q^{(1,3)}$ and $Q^{(1,5)}$ from [12] as weighted t -designs Q_{S^3} and $Q_{S_1^3}$, we checked numerically that the resulting quadrature rule $Q_{SU(3)}$ is again a weighted t -design over $SU(3)$, for $t \leq 3$. The latter observation drove us to investigate a procedure in more detail for constructing weighted t -design rules over $SU(N)$, for arbitrary positive integers N and t . This procedure is based on a generalization of the mapping Φ_3 as stated above and relies on the correspondence⁴ between $SU(N)$ and $\times_{j=1}^{N-1} S^{2j+1}$. This new construction of quadrature rules over $SU(N)$ is subject of current research by the authors, but the potential applications of this new method exceed the scope of this article and will be not reported at this point.

Note that the procedure above is not the only way of writing integrals over $SU(N)$ as an integral over spheres. For instance, using the eigenvalue decomposition of $SU(N)$ we obtain integrals over products of $U(1)$. However, it should be noted that the eigenvalue decomposition is not an isomorphism and, thus, a functional determinant will appear (which in itself is a polynomial). In other words, the polynomial degree of the integrand will increase. Nonetheless this is a viable approach to obtain polynomial exactness, and using the points in Eq. (19) yields a method equivalent to [17].

IV. NUMERICAL RESULTS

In this section we will provide a comparison of the evaluation of the partition function Z and the chiral condensate χ using MC-MC and our new polynomially exact integration rules. First we will concentrate on the partition function Z . We will have a short look at the behavior of the analytic values of Z before comparing them to the quadrature results of Z using the Monte Carlo and polynomially exact method in terms of a relative error. To present the real power of the polynomially exact method, we will show computational results for two different floating point number precisions. Then we will investigate the relative error behavior of the chiral condensate. Since we compute the relative error as the deviation of the quadrature result from the computation using analytic formulas, we explicitly differentiate these ways of computation in the following using the terms $Z_{\text{quadrature}}$ and Z_{analytic} .

As stated above, for the here-considered model both Z and χ can be computed analytically for the groups $U(N)$ and $SU(N)$. In particular, the expression of the partition functions in Theorem 2 for $SU(N)$ can be related to the one for $U(N)$ through

⁴Induction over $SU(j)$ being a principal $SU(j-1)$ bundle over S^{2j-1} [see Eq. (22.18) of [16]] and $SU(2) \cong S^3$.

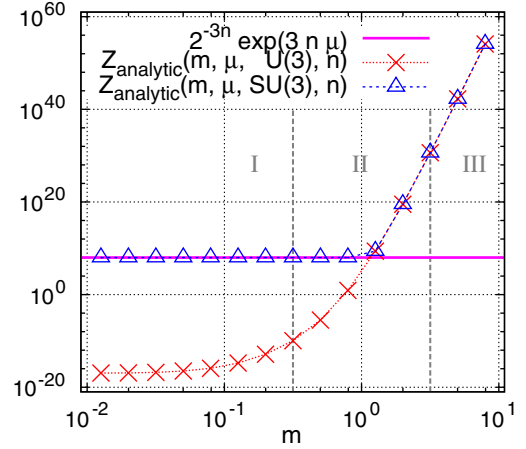


FIG. 2. Order of the quadrature-rule point evaluation of the partition function integrand, $(2^{-n} e^{n\mu})^3$, see (6), compared to the analytic values of the partition functions for $U(3)$ and $SU(3)$ (see Theorem 2), using $n = 20$, $\mu = 1$. As discussed in the paper, the ratio $Z_{\text{analytic}}/2^{-3n} e^{3n\mu}$ determines the relative errors of the partition function and the chiral condensate to a large extent. In particular, we identify three regions (I, II, and III) in which the relative error exhibits qualitatively different behavior. (These computations were performed with 1024-bit floating point arithmetic.)

$$\begin{aligned} Z_{\text{analytic}}(m, \mu, SU(N), n) &= Z_{\text{analytic}}(m, \mu, U(N), n) + c_2^N + c_3^N \\ &= Z_{\text{analytic}}(m, \mu, U(N), n) \\ &\quad + \begin{cases} 2^{1-Nn} \cosh(Nn\mu), & n \in 2\mathbb{N} \\ -2^{1-Nn} \sinh(Nn\mu), & n \in 2\mathbb{N} - 1. \end{cases} \end{aligned} \quad (25)$$

We note that for $U(N)$ the partition function smoothly approaches a much smaller value than $c_2^N + c_3^N$ when decreasing the mass parameter m , while for $SU(N)$ it approaches a constant near $c_2^N + c_3^N$ as given in Theorem 2; see also Corollary 1. The behavior of $Z_{\text{analytic}}(m, \mu, G, n)$ as a function of the mass parameter m for $G \in \{U(3), SU(3)\}$, $n = 6$, $\mu = 1$ is shown in Fig. 2 and there we can clearly see the different behaviors of Z_{analytic} for $U(3)$ and $SU(3)$ for $m \searrow 0$.

For the groups $U(N)$ and $SU(N)$ each point evaluation of the quadrature rule is of order $O(2^{-Nn} e^{Nn\mu})$; that is, a double precision computation cannot resolve values below $10^{-16} 2^{-Nn} e^{Nn\mu}$. Since the behavior of the partition function in comparison to the constant $c_2^N + c_3^N$ will be important in order to understand the relative error $|Z_{\text{quadrature}} - Z_{\text{analytic}}|/Z_{\text{analytic}}$, we also show the value of $|c_2^3 + c_3^3| \approx 2^{-3n} e^{3n\mu}$ in Fig. 2 (see discussion at the end of Sec. II above, as well) for the examples of $U(3)$ and $SU(3)$. In Fig. 2, we furthermore distinguished three regions with different behavior, indicated in the following as region I, II, and III.

Let us first discuss the group $U(3)$. For large values of m (region III) $2^{-3n} e^{3n\mu}$ is negligible compared to Z_{analytic} . We therefore expect a small deviation of $Z_{\text{quadrature}}$ from Z_{analytic} and hence a small relative error. On the other hand, for small values of m (region I) Z_{analytic} becomes much smaller than $2^{-3n} e^{3n\mu}$ and we expect a significant relative error due to rounding errors. There is also a transition regime in m (region II) in which the values of Z_{analytic} and $2^{-3n} e^{3n\mu}$ have the same order of magnitude. Hence, we expect a significant increase in the relative error while decreasing m , but the smooth behavior of Z_{analytic} for $U(3)$ suggests that there will be a similarly smooth increase of the relative error as a function of m . As we will discuss below, this expectation is indeed verified in our numerical tests.

In the $SU(3)$ case, we have the additional constant $c_2^3 + c_3^3$ which, for small m , is significantly larger than $Z_{\text{analytic}}(U(3))$, see (25). Looking at Fig. 2, we expect a relative error similar to the $U(3)$ case in region III. In region I, though, the relative error should be much less now due to the fact that the analytic value and order of magnitude of each point evaluation are closer together than in the $U(3)$ case. In the transition region II, the behavior may be different from $U(3)$ as well, although this is not deduced from the figure *per se* but from the differences in the formulas of Z_{analytic} (25). There, the m -dependent term of Z_{analytic} , the constant $c_2^N + c_3^N$, and the point evaluation in the quadrature rules are of the same order of magnitude $O(2^{-Nn} e^{Nn\mu})$. Thus, this additional term $c_2^N + c_3^N$, not present at $U(N)$, could lead to competing effects for the relative error and, hence, an irregular behavior of the relative error (at least in the MC-MC case).

Let us now move on to our numerical experiments. In Fig. 3, we compare the quadrature rule

$$\begin{aligned} Z_{\text{quadrature}}^{\text{MCMC}}(m, \mu, G, n) \\ = \int_G \det \mathfrak{D} h_G \approx \frac{1}{\#Q_G} \sum_{k=1}^{\#Q_G} \det \mathfrak{D}(U_k) \end{aligned} \quad (26)$$

where each U_k is chosen randomly in G (uniformly with respect to the Haar measure) and the polynomially exact version

$$\begin{aligned} Z_{\text{quadrature}}^{\text{poly. exact}}(m, \mu, G, n) &= \int_G \det \mathfrak{D} h_G \\ &\approx \frac{1}{\#Q_G} \sum_{V \in Q_G} \det \mathfrak{D}(VU_1) \end{aligned} \quad (27)$$

where U_1 is the U_1 sampled in the nonexact version in (26).⁵ Here, we chose

⁵Any $U_1 \in G$ would be perfectly fine; in fact, choosing the identity for U_1 would be a good canonical choice. However, we chose U_1 randomly (uniformly with respect to the Haar measure) in order to approximate the error.

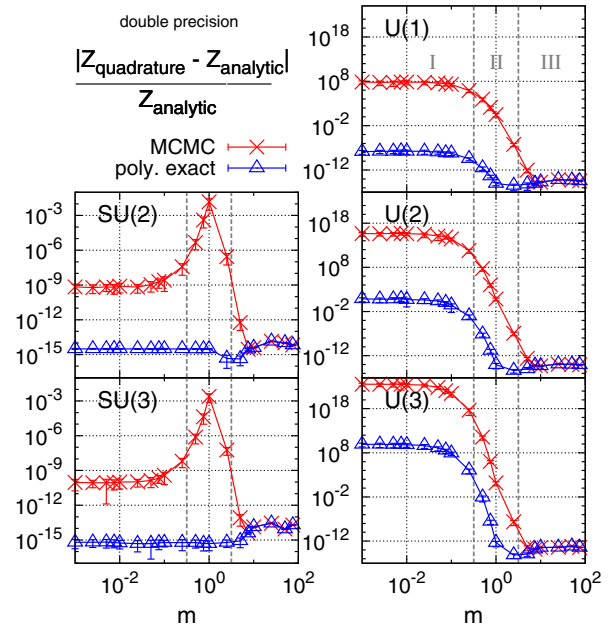


FIG. 3. Comparison of the relative error of the used methods, namely the polynomially exact and Monte Carlo quadrature rules to calculate the partition function Z for $SU(2)$ and $SU(3)$ (left column, top to bottom), and $U(1)$, $U(2)$, and $U(3)$ (right column, top to bottom) with $n = 20$, $\mu = 1$, $m \in [0.001, 100]$. Averages and standard deviations (error bars) have been computed from 50 independent computations. Here we used double precision to carry through the numerical calculations. The different behaviors of the relative error regarding different values of m are divided into regions I, II and III, corresponding to Fig. 2.

$$Q_G = \begin{cases} \{e^{\frac{2\pi i k}{4}}; k \in \mathbb{Z}_4\}, & G = U(1) \\ \Phi[Q_{S^3}], & G = SU(2) \\ \{e^{\frac{2\pi i k}{4}} U; k \in \mathbb{Z}_4, U \in \Phi[Q_{S^3}]\}, & G = U(2) \\ \Phi_3[Q_{S^5} \times Q_{S^3}], & G = SU(3) \\ \{e^{\frac{2\pi i k}{4}} U; k \in \mathbb{Z}_4, U \in \Phi_3[Q_{S^5} \times Q_{S^3}]\}, & G = U(3) \end{cases} \quad (28)$$

where Q_{S^3} and Q_{S^5} are randomized fully symmetric rules of polynomial degree 3 on S^3 and S^5 according to [12]. To obtain the error estimates, we repeated each numerical experiment 50 times.

Figure 3 shows the relative error of the partition function computed according to (26) and (27). The same m -regions (I, II, and III), as shown in Fig. 2, are indicated here as well and we can see that the behavior of the relative error is quite distinct for each of the three regions. For large values of m (region III), both methods operate with double precision as expected from the discussion above.

Regarding regions I and II, we will consider the $U(N)$ case first. As we move to smaller m , we enter the transition region (II) and for $U(N)$ the relative error increases significantly but in a smooth way. As shown in Fig. 2,

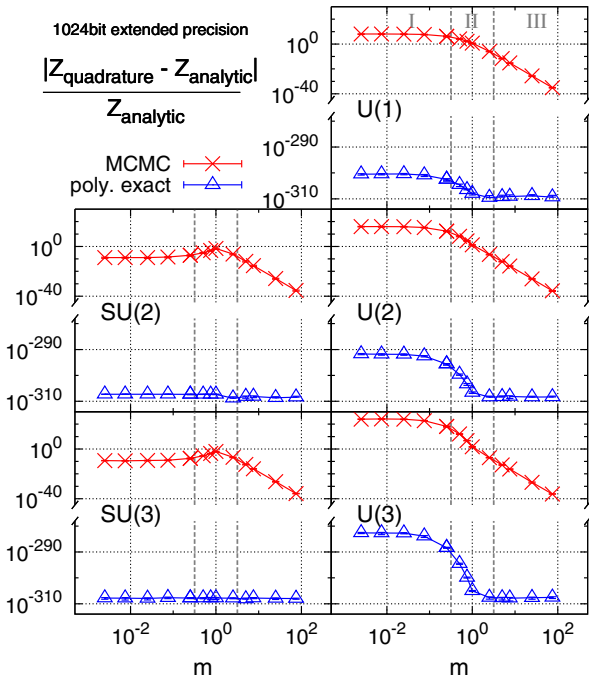


FIG. 4. Comparison of the relative error as shown in Fig. 3 but here using 1024-bit extended floats. Averages and standard deviations (error bars) have been computed from 50 independent computations for $U(1)$, $U(2)$, and $SU(2)$, and from 10 independent computations for $SU(3)$ and $U(3)$. Again $n = 20$, $\mu = 1$, and $m \in [0.001, 100]$ are used.

for very small values of m (region I) $Z_{\text{analytic}}(m, \mu, U(N), n)$ is significantly smaller than $2^{-Nn} e^{Nn\mu}$; hence, $Z_{\text{analytic}}(m, \mu, U(N), n)$ is negligible compared to the machine error and we observe large relative errors in region I of Fig. 3. Note that the polynomially exact computation still sums values of magnitude $2^{-Nn} e^{Nn\mu}$; i.e., the relative error of the exact method cannot be below 10^{-16} times the error of the nonexact method which is, indeed, what we see in Fig. 3. Returning to Fig. 2 and the $U(N)$ discussion above, the observed smooth increase of the relative error in region II matches our expectations.

In the $SU(N)$ case, the relative error is comparable to the $U(N)$ case in regions I and III; we simply obtain smaller errors in region I since $2^{-Nn} e^{Nn\mu}$ does not dominate Z_{analytic} as is the case for $U(N)$. However, in the transition region II of Fig. 3, we can see a rather irregular behavior, the possibility for which to occur we already mentioned in the discussion of Z_{analytic} above. This can be attributed to the fact that the mass-dependent term of $Z_{\text{analytic}}(m, \mu, U(N), n)$ and the constant $c_2^N + c_3^N$, see (25), as well as the point evaluations in $Z_{\text{quadrature}}$, are of the same order of magnitude. Hence neither term can suppress the error of the other, which we interpret as the cause of the peak in the relative error.

Figure 4 shows the same comparison as Fig. 3 but computations were performed with 1024-bit floating

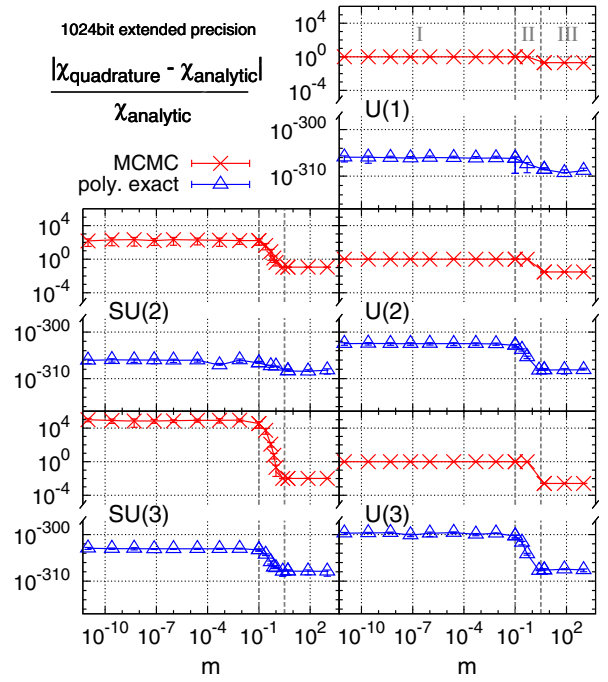


FIG. 5. Comparison of the relative error of the chiral condensate $\chi = \partial_m \ln Z$ using polynomially exact and Monte Carlo quadrature rules for $SU(2)$ and $SU(3)$ (left column, top to bottom), and $U(1)$, $U(2)$, and $U(3)$ (right column, top to bottom) with $n = 8$, $\mu = 1.0$, and $m \in [10^{-11}, 10^3]$. We use 1024-bit extended floats. Averages and standard deviations (error bars) have been computed from 50 independent computations for $SU(2)$, $U(1)$, and $U(2)$ and from 5 for $SU(3)$ and $U(3)$. The different behaviors of the error regarding different values of m are divided into regions I, II, and III.

point arithmetic,⁶ i.e., approximately 307-digit precision. Again, we observe that the polynomially exact method operates on machine precision (as to be expected). The averages and standard deviations of the relative error were computed from 50 independent computations for $G \in \{U(1), SU(2), U(2)\}$ and from 10 independent computations for $G \in \{SU(3), U(3)\}$. All computations were performed on an IBM laptop in less than an hour.⁷ The behavior of the relative error, for both, Monte Carlo and polynomially exact method, is very similar to the double precision case in Fig. 3. Note that the polynomially exact integration always leads to machine precision results even in this extreme case of 1024-bit precision, whereas the relative error of the MC-MC results does not notably decrease in regions I and II when replacing double precision floats in Fig. 3 with 1024-bit extended floats in Fig. 4.

⁶These are 1024 mantissa bits; double precision (about 15-digit precision) corresponds to 53 bits.

⁷For $SU(3)$ and $U(3)$ only, runtime was considerably longer than a few minutes.

In general, we observe in Figs. 3 and 4 that the polynomially exact quadrature rule always provides machine error results.

In order to test our new polynomially exact method against an actual physical observable, Fig. 5 shows the comparison of the relative error of the chiral condensate (again using 1024-bit extended floats). The analytic values of the chiral condensate have been obtained through symbolic differentiation of the formulas in Theorem 2; the numerical values by symbolic differentiation of (6). We observe that the relative error follows the trend we have already seen for the partition function in the three different regions.⁸

Let us discuss the relative error in Fig. 5 in a bit more detail. A first observation is that the polynomially exact method operates on the level of machine precision and, as such, reduces the relative error by (many) orders of magnitude for all values of m . Even more interesting and striking is the size of the relative error of the chiral condensate in the small- m region. As pointed out in [7], in this region of parameter space there is a severe sign problem. Indeed, for the MC-MC method the relative error becomes $O(1)$ for sufficiently small m ; i.e., no statistically significant result for the chiral condensate can be obtained with standard MC-MC calculations. [In Fig. 5, this behavior can only be seen for $U(N)$ but it is also present and was observed by us for $SU(N)$ for m -values smaller than the ones shown here.⁹] This is a clear manifestation of the infamous sign problem.

In contrast, our polynomially exact method again provides results on machine precision. Thus, the polynomially exact method completely overcomes the sign problem and can lead to very accurate results even in regions where MC-MC computations are unfeasible.

V. CONCLUSION

In this work, we have developed and tested a new integration method for the groups $U(N)$ and $SU(N)$. As a major outcome of our work, we could in fact provide a numerical verification that the method developed here leads to polynomial exactness of the integration for $N \leq 3$. We have applied the method to the one-dimensional QCD with a chemical potential where for certain values of the action parameters a sign

problem appears with MC-MC methods. Using the groups $U(1), U(2), U(3)$ and $SU(2), SU(3)$ we have demonstrated that even for cases when the sign problem is most severe, the chiral condensate of this model can be computed to arbitrary precision with the new method. In contrast, standart MC-MC methods show large $O(1)$ relative errors and do not give any statistically significant result. For this comparison, we even went to 1024-bit extended precision and were able to show that our new method still achieves results on the level of machine precision. We therefore conclude that our polynomially exact integration method can completely avoid the sign problem. Furthermore, it is important to point out that it also leads to errors reduced by orders of magnitude compared to MC-MC even in regions of parameter space where no sign problem occurs.

The fact that our new integration method overcomes the sign problem and leads in general to errors reduced by orders of magnitude in the one-dimensional QCD considered here is certainly a very promising finding and stands as a result by itself. However, this benchmark model can only be regarded as a toy example. It will be necessary to demonstrate that the method can also be applied in higher dimensions. To this end, we are presently considering the Schwinger model as an example of a quantum field theory in two dimensions.

In addition, so far we do not have proof yet of the polynomial exactness for the groups $U(N)$ and $SU(N)$ with general N . Although we are very confident that our integration method leads to polynomial exactness for general N , we are working on a proof to substantiate this statement.

ACKNOWLEDGMENTS

The authors wish to express their gratitude to Prof. Andreas Griewank for inspiring comments and conversations, which helped to develop the work in this article. H. L. and J. V. acknowledge financial support by the Projects No. JA 674/6-1 and No. GR 705/13, funded by the Deutsche Forschungsgemeinschaft.

APPENDIX A: PROOF OF THEOREM 1

Let

$$Y = \begin{pmatrix} A & B \\ C & D \end{pmatrix} \quad (\text{A1})$$

be a block decomposition where A and D are square matrices and A is invertible. Then,

$$\det Y = \det A \det (D - CA^{-1}B). \quad (\text{A2})$$

Here, we are considering matrices of the form

⁸Here, the range of the regions differs from before.

⁹The larger relative error $> O(1)$ for $SU(N)$ at small m seen here is due to $\lim_{m \searrow 0} \mathcal{Z}_{\text{analytic}}(m, \mu, SU(N), n) = 0$, because $\lim_{m \searrow 0} \partial_m \mathcal{Z}_{\text{analytic}}(m, \mu, SU(N), n) = 0$ and $\lim_{m \searrow 0} \mathcal{Z}_{\text{analytic}}(m, \mu, SU(N), n) \neq 0$. Thus, the analytic result for some small m is already at machine precision while the quadrature result is not, such that division by this small machine precision number yields a value which can be larger than one.

$$X = \begin{pmatrix} m_1 & \frac{e^\mu}{2} U_1 & & & \frac{e^{-\mu}}{2} U_n^* \\ -\frac{e^{-\mu}}{2} U_1^* & m_2 & \frac{e^\mu}{2} U_2 & & \\ & -\frac{e^{-\mu}}{2} U_2^* & m_3 & \frac{e^\mu}{2} U_3 & \\ & & \ddots & \ddots & \ddots \\ & & & -\frac{e^{-\mu}}{2} U_{n-2}^* & m_{n-1} & \frac{e^\mu}{2} U_{n-1} \\ -\frac{e^\mu}{2} U_n & & & & -\frac{e^{-\mu}}{2} U_{n-1}^* & m_n \end{pmatrix} \tag{A3}$$

where all m_i are positive. Choosing A to be the m_1 block in X , we obtain

$$D = \begin{pmatrix} m_2 & \frac{e^\mu}{2} U_2 & & & \\ -\frac{e^{-\mu}}{2} U_2^* & m_3 & \frac{e^\mu}{2} U_3 & & \\ & -\frac{e^{-\mu}}{2} U_3^* & m_4 & \frac{e^\mu}{2} U_4 & \\ & & \ddots & \ddots & \ddots \\ & & & -\frac{e^{-\mu}}{2} U_{n-2}^* & m_{n-1} & \frac{e^\mu}{2} U_{n-1} \\ & & & & -\frac{e^{-\mu}}{2} U_{n-1}^* & m_n \end{pmatrix} \tag{A4}$$

and

$$-CA^{-1}B = \frac{-1}{m_1} \begin{pmatrix} -\frac{1}{4} & 0 & -\frac{e^{-2\mu}}{4} U_1^* U_n^* \\ 0 & 0 & 0 \\ -\frac{e^{2\mu}}{4} U_n U_1 & 0 & -\frac{1}{4} \end{pmatrix}. \tag{A5}$$

In other words, $D - CA^{-1}B$ is of the initial form again and

$$\det X = m_1^N \det(D - CA^{-1}B) \tag{A6}$$

$$= \det \begin{pmatrix} m_2 + \frac{1}{4m_1} & \frac{e^\mu}{2} U_2 & & & \frac{2^{-2}e^{-2\mu}}{m_1} U_1^* U_n^* \\ -\frac{e^{-\mu}}{2} U_2^* & m_3 & \frac{e^\mu}{2} U_3 & & \\ & -\frac{e^{-\mu}}{2} U_3^* & m_4 & \frac{e^\mu}{2} U_4 & \\ & & \ddots & \ddots & \ddots \\ & & & -\frac{e^{-\mu}}{2} U_{n-2}^* & m_{n-1} & \frac{e^\mu}{2} U_{n-1} \\ \frac{2^{-2}e^{2\mu}}{m_1} U_n U_1 & & & & -\frac{e^{-\mu}}{2} U_{n-1}^* & m_n + \frac{1}{4m_1} \end{pmatrix}. \tag{A7}$$

Let $U_0 := U_n, \tilde{m}_1 := m_1,$

$$\forall j \in [2, n-1] \cap \mathbb{N}: \tilde{m}_j := m_j + \frac{1}{4\tilde{m}_{j-1}}, \tag{A8}$$

and

$$\tilde{m}_n := m_n + \frac{1}{4\tilde{m}_{n-1}} + \sum_{j=1}^{n-1} \frac{(-1)^{j+1} 2^{-2j}}{\tilde{m}_j \prod_{k=1}^{j-1} \tilde{m}_k^2}. \tag{A9}$$

Then, we obtain inductively

$$\det X = \prod_{j=1}^{n-3} \tilde{m}_j^N \det \begin{pmatrix} \tilde{m}_{n-2} & \frac{e^\mu}{2} U_{n-2} & \frac{2^{-(n-2)} e^{-(n-2)\mu}}{\prod_{j=1}^{n-3} \tilde{m}_j} \left(\prod_{j=1}^{n-2} U_{j-1} \right)^* \\ -\frac{e^{-\mu}}{2} U_{n-2}^* & m_{n-1} & \frac{e^\mu}{2} U_{n-1} \\ \frac{(-1)^{n-2} 2^{-(n-2)} e^{(n-2)\mu}}{\prod_{j=1}^{n-3} \tilde{m}_j} \prod_{j=1}^{n-2} U_{j-1} & -\frac{e^{-\mu}}{2} U_{n-1}^* & m_n + \sum_{j=1}^{n-3} \frac{(-1)^j 2^{-2j}}{\tilde{m}_j \prod_{k=1}^{j-1} \tilde{m}_k^2} \end{pmatrix} \quad (\text{A10})$$

$$= \prod_{j=1}^{n-1} \tilde{m}_j^N \det \left(\tilde{m}_n + \frac{(-1)^n 2^{-n} e^{n\mu}}{\prod_{j=1}^{n-1} \tilde{m}_j} \prod_{j=1}^n U_{j-1} + \frac{2^{-n} e^{-n\mu}}{\prod_{j=1}^{n-1} \tilde{m}_j} \left(\prod_{j=1}^n U_{j-1} \right)^* \right) \quad (\text{A11})$$

which finally yields

$$\det X = \det \left(\prod_{j=1}^n \tilde{m}_j + (-1)^n 2^{-n} e^{n\mu} \prod_{j=1}^n U_{j-1} + 2^{-n} e^{-n\mu} \left(\prod_{j=1}^n U_{j-1} \right)^* \right). \quad (\text{A12})$$

APPENDIX B: PROOF OF THEOREM 2

Note that the $U(1)$ case is trivial. Hence, we will start considering $U(N)$ with $N \geq 2$ and use the notations

$$U_{ij}^* := (U^*)_{ij} \quad (\text{B1})$$

and

$$\forall p \in \mathbb{N}_0 \quad \forall I, \quad J \in \mathbb{N}_{\leq N}^p: U_{IJ} := \prod_{k=0}^{p-1} U_{I_k J_k} \wedge U_{IJ}^* := \prod_{k=0}^{p-1} (U^*)_{I_k J_k}. \quad (\text{B2})$$

Furthermore, we set $\forall p, q \in \mathbb{N}_0 \quad \forall I, J \in \mathbb{N}_{\leq N}^p \quad \forall K, L \in \mathbb{N}_{\leq N}^q$,

$$\langle I, J | K, L \rangle := \int_{U(N)} U_{IJ}^* U_{KL} dh_{U(N)}(U) \quad (\text{B3})$$

and use abbreviations for empty sets or singletons similar to

$$\langle 0, 1 | \rangle := \langle (0), (1) | (0), (1) \rangle. \quad (\text{B4})$$

The following identities are well known (cf., e.g., [18]):

- (i) $p \neq q \Rightarrow \langle I, J | K, L \rangle = 0$
- (ii) $\langle | \rangle = 1$
- (iii) $\langle i, j | k, l \rangle = \frac{\delta_{ij} \delta_{kl}}{N}$.

For $N = 2$, we may expand the determinant in

$$\int_{U(2)} \det \mathfrak{D} dh_{U(2)} = \int_{U(2)} \det (c_1 + c_2 U^* + c_3 U) dh_{U(2)}(U) \quad (\text{B5})$$

$$= \int_{U(2)} \det \begin{pmatrix} c_1 + c_2 U_{00}^* + c_3 U_{00} & c_2 U_{01}^* + c_3 U_{01} \\ c_2 U_{10}^* + c_3 U_{10} & c_1 + c_2 U_{11}^* + c_3 U_{11} \end{pmatrix} dh_{U(2)}(U) \quad (\text{B6})$$

directly and, using the identities above, we obtain

$$\int_{U(2)} \det \mathfrak{D} dh_{U(2)} = c_1^2 - c_2 c_3. \quad (\text{B7})$$

Similarly, we can expand the determinant in

$$\int_{U(3)} \det \begin{pmatrix} c_1 + c_2 U_{00}^* + c_3 U_{00} & c_2 U_{01}^* + c_3 U_{01} & c_2 U_{02}^* + c_3 U_{02} \\ c_2 U_{10}^* + c_3 U_{10} & c_1 + c_2 U_{11}^* + c_3 U_{11} & c_2 U_{12}^* + c_3 U_{12} \\ c_2 U_{20}^* + c_3 U_{20} & c_2 U_{21}^* + c_3 U_{21} & c_1 + c_2 U_{22}^* + c_3 U_{22} \end{pmatrix} dh_{U(3)}(U) \quad (\text{B8})$$

using Sarrus's rule, which yields

$$\int_{U(3)} \det \mathfrak{D}h_{U(3)} = c_1^3 - 2c_1 c_2 c_3 \quad (\text{B9})$$

using the identities above.

For $SU(N)$, we have

- (i) $p \neq q \Rightarrow \langle I, J | K, L \rangle = 0$
- (ii) $\langle | \rangle = 1$
- (iii) $\langle i, j | k, l \rangle = \frac{\delta_{ij} \delta_{kl}}{N}$
- (iv) $\langle (i, j), (k, l) | \rangle = \langle | (i, j), (k, l) \rangle = -\frac{(-1)^{\delta_{ik}}}{2} = \frac{(-1)^{\epsilon_{ik}}}{2}$
in $SU(2)$
- (v) $\langle | (i, j, k), (l, m, n) \rangle = \langle (i, j, k), (l, m, n) | \rangle = \frac{\epsilon_{ijk} \epsilon_{lmn}}{6}$
in $SU(3)$.

Hence [analogous to the $U(N)$ computations],

$$\int_{SU(2)} \det \mathfrak{D}h_{SU(2)} = c_1^2 + c_2^2 - c_2 c_3 + c_3^2 \quad (\text{B10})$$

and

$$\int_{SU(3)} \det \mathfrak{D}h_{SU(3)} = c_1^3 - 2c_1 c_2 c_3 + c_2^3 + c_3^3. \quad (\text{B11})$$

APPENDIX C: PROOF OF COROLLARY 1

By induction, we note for $2j < n$

$$\lim_{m \searrow 0} \frac{\tilde{m}_{2j-1}}{jm} = 1 \quad \text{and} \quad \lim_{m \searrow 0} \frac{\tilde{m}_{2j}}{\frac{1}{4jm}} = 1. \quad (\text{C1})$$

This is trivially true for $\tilde{m}_1 = m$ and $\tilde{m}_2 = m + \frac{1}{4m}$. Then, we observe for $j > 1$

$$\lim_{m \searrow 0} \frac{\tilde{m}_{2j-1}}{jm} = \lim_{m \searrow 0} \frac{m + \frac{1}{4\tilde{m}_{2j-2}}}{jm} = \lim_{m \searrow 0} \frac{1}{j} + \frac{1}{4\tilde{m}_{2j-2} jm} \quad (\text{C2})$$

$$= \lim_{m \searrow 0} \frac{1}{j} + \frac{\frac{1}{4 \frac{1}{4(j-1)m}}}{jm} \quad (\text{C3})$$

$$= \frac{1}{j} + \frac{j-1}{j} = 1 \quad (\text{C4})$$

and

$$\lim_{m \searrow 0} \frac{\tilde{m}_{2j}}{\frac{1}{4jm}} = \lim_{m \searrow 0} \frac{m + \frac{1}{4\tilde{m}_{2j-1}}}{\frac{1}{4jm}} = \lim_{m \searrow 0} 4jm^2 + \frac{jm}{\tilde{m}_{2j-1}} = 1. \quad (\text{C5})$$

Thus, we obtain

$$\lim_{m \searrow 0} \tilde{m}_k \tilde{m}_{k+1} = \begin{cases} \lim_{m \searrow 0} \frac{\tilde{m}_k \tilde{m}_{k+1}}{jm \frac{1}{4jm}}, & k = 2j - 1 \\ \lim_{m \searrow 0} \frac{\tilde{m}_k \tilde{m}_{k+1}}{\frac{1}{4jm} (j+1)m \frac{1}{4jm}}, & k = 2j \end{cases} = \begin{cases} \frac{1}{4}, & k = 2j - 1 \\ \frac{j+1}{4j}, & k = 2j \end{cases} \quad (\text{C6})$$

and for $n \in 2\mathbb{N}$

$$\lim_{m \searrow 0} c_1 = \lim_{m \searrow 0} m \tilde{m}_n \prod_{j=1}^{\frac{n}{2}-1} \underbrace{\tilde{m}_{2j} \tilde{m}_{2j+1}}_{\rightarrow \frac{j+1}{4j}} \quad (\text{C7})$$

$$= 2^{1-n} n \lim_{m \searrow 0} m \tilde{m}_n \quad (\text{C8})$$

$$= 2^{1-n} n \lim_{m \searrow 0} m \left(m + \frac{1}{4\tilde{m}_{n-1}} + \sum_{j=1}^{n-1} \frac{(-1)^{j+1} 4^{-j}}{m \prod_{k=1}^{j-1} \tilde{m}_k \tilde{m}_{k+1}} \right) \quad (\text{C9})$$

$$= 2^{1-n} n \lim_{m \searrow 0} \left(\frac{\frac{n}{2} m}{4\tilde{m}_{n-1}} \frac{2}{n} + \sum_{j=1}^{n-1} \frac{(-1)^{j+1} 4^{-j}}{\prod_{k=1}^{j-1} \tilde{m}_k \tilde{m}_{k+1}} \right) \quad (\text{C10})$$

$$= 2^{1-n} n \left(\frac{1}{2n} + \lim_{m \searrow 0} \sum_{j=1}^{\frac{n}{2}} \frac{(-1)^{(2j-1)+1} 4^{-(2j-1)}}{\prod_{k=1}^{(2j-1)-1} \tilde{m}_k \tilde{m}_{k+1}} + \sum_{j=1}^{\frac{n}{2}-1} \frac{(-1)^{2j+1} 4^{-2j}}{\prod_{k=1}^{2j-1} \tilde{m}_k \tilde{m}_{k+1}} \right) \quad (\text{C11})$$

$$= 2^{1-n} n \left(\frac{1}{2n} + \sum_{j=1}^{\frac{n}{2}} \frac{4^{1-2j}}{\prod_{k=1}^{2(j-1)} \lim_{m \searrow 0} \tilde{m}_k \tilde{m}_{k+1}} - \sum_{j=1}^{\frac{n}{2}-1} \frac{4^{-2j}}{\prod_{k=1}^{2j-1} \lim_{m \searrow 0} \tilde{m}_k \tilde{m}_{k+1}} \right) \quad (\text{C12})$$

$$= 2^{1-n} n \left(\frac{1}{2n} + \sum_{j=1}^{\frac{n}{2}} \frac{4^{1-2j}}{4^{2-2j} \prod_{k=1}^{j-1} \frac{k+1}{k}} - \sum_{j=1}^{\frac{n}{2}-1} \frac{4^{-2j}}{4^{1-2j} \prod_{k=1}^{j-1} \frac{k+1}{k}} \right) \quad (\text{C13})$$

$$= 2^{1-n} n \left(\frac{1}{2n} + \sum_{j=1}^{\frac{n}{2}} \frac{1}{4j} - \sum_{j=1}^{\frac{n}{2}-1} \frac{1}{4j} \right) \quad (\text{C14})$$

$$= 2^{1-n} n \left(\frac{1}{2n} + \frac{1}{2n} \right) \quad (\text{C15})$$

$$= 2^{1-n}. \quad (\text{C16})$$

Similarly, for $n \in 2\mathbb{N} - 1$,

$$\lim_{m \searrow 0} c_1 = \lim_{m \searrow 0} \tilde{m}_n \prod_{j=1}^{\frac{n-1}{2}} \underbrace{\tilde{m}_{2j-1} \tilde{m}_{2j}}_{\rightarrow \frac{1}{4}} \quad (\text{C17})$$

$$= 2^{1-n} \lim_{m \searrow 0} \left(m + \frac{4^{\frac{n-1}{2}} m}{4^{\frac{m_{n-1}}{4^{\frac{n-1}{2}} m}}} + \sum_{j=1}^{\frac{n-1}{2}} \frac{4^{1-2j}}{m \prod_{k=1}^{2j-2} \tilde{m}_k \tilde{m}_{k+1}} - \sum_{j=1}^{\frac{n-1}{2}} \frac{4^{-2j}}{m \prod_{k=1}^{2j-1} \tilde{m}_k \tilde{m}_{k+1}} \right) \quad (\text{C18})$$

$$= 2^{1-n} \lim_{m \searrow 0} \left(\sum_{j=1}^{\frac{n-1}{2}} \frac{4^{1-2j}}{4^{2-2j} j m} - \sum_{j=1}^{\frac{n-1}{2}} \frac{4^{-2j}}{4^{1-2j} j m} \right) \quad (\text{C19})$$

$$= 0. \quad (\text{C20})$$

Finally, the asserted identities for $Z(m, \mu, G, n)$ with $G \in \{U(1), SU(2), U(2), SU(3), U(3)\}$ are a trivial corollary substituting $\lim_{m \searrow 0} c_1$ into the formulas given in Theorem 2.

-
- [1] M. Troyer and U.-J. Wiese, Computational Complexity and Fundamental Limitations to Fermionic Quantum Monte Carlo Simulations, *Phys. Rev. Lett.* **94**, 170201 (2005).
- [2] C. Gattringer and K. Langfeld, Approaches to the sign problem in lattice field theory, *Int. J. Mod. Phys. A*, **31**, 1643007 (2016).
- [3] D. Sexty, New algorithms for finite density QCD., *Proc. Sci.*, LATTICE2014 (2014) 016.
- [4] C.. Gattringer, New developments for dual methods in lattice field theory at non-zero density, *Proc. Sci.*, LATTICE2013 (2014) 002.
- [5] K. Jansen, H. Leovey, A. Ammon, A. Griewank, and M. Muller-Preussker, Quasi-Monte Carlo methods for lattice systems: A first look, *Comput. Phys. Commun.* **185**, 948 (2014).
- [6] A. Ammon, A. Genz, T. Hartung, K. Jansen, H. Leövey, and J. Volmer, On the efficient numerical solution of lattice systems with low-order couplings, *Comput. Phys. Commun.* **198**, 71 (2016).
- [7] L. Ravagli and J. J. M. Verbaarschot, QCD in one dimension at nonzero chemical potential, *Phys. Rev. D* **76**, 054506 (2007).
- [8] G. Aarts and K. Splittorff, Degenerate distributions in complex Langevin dynamics: One-dimensional QCD at finite chemical potential, *J. High Energy Phys.* **08** (2010) 017.
- [9] E.-M. Ilgenfritz and J. Kripfganz, Dynamical fermions at nonzero chemical potential and temperature: Mean field approach, *Z. Phys. C* **29**, 79 (1985).
- [10] J. Bloch, F. Bruckmann, and T. Wettig, Subset method for one-dimensional QCD, *J. High Energy Phys.* **10** (2013) 140.
- [11] J. Bloch, F. Bruckmann, and T. Wettig, Sign problem and subsets in one-dimensional QCD, *Proc. Sci.*, LATTICE2013 (2014) 194.
- [12] A. Genz, Fully symmetric interpolatory rules for multiple integrals over hyper-spherical surfaces, *J. Comput. Appl. Math.* **157**, 187 (2003).
- [13] H. Abbaspour and M. Moskowitz, *Basic Lie Theory* (World Scientific, Singapore, 2007).
- [14] P. Delsarte, J. M. Goethals, and J. J. Seidel, Spherical codes and designs, *Geometriae Dedicata* **6**, 363 (1977).
- [15] I. H. Sloan and R. S. Womersley, Good approximation on the sphere, with application to geodesy and the scattering of sound, *J. Comput. Appl. Math.* **149**, 227 (2002).
- [16] T. Frankel, *The Geometry of Physics: An Introduction*, 3rd ed. (Cambridge University Press, Cambridge, England, 2012).
- [17] J. Bloch, F. Bruckmann, M. Kieburg, K. Splittorff, and J. J. M. Verbaarschot, Subsets of configurations and canonical partition functions, *Phys. Rev. D* **87**, 034510 (2013).
- [18] C. Gattringer and C. B. Lang, Quantum chromodynamics on the lattice, *Lect. Notes Phys.* **788**, 1 (2010).